Investigation of Ni Sorption on Pyrophyllite: An XAFS Study

ANDRE M. SCHEIDEGGER,*,† GERALDINE M. LAMBLE,‡ AND DONALD L. SPARKS†

Department of Plant and Soil Sciences, University of Delaware, Newark, Delaware 19717-1303, and Building 510E, Brookhaven National Laboratory, Upton, New York 11973

Sorption reactions at the solid−water interface decrease solute mobility and often control the fate, bioavailability, and transport of metal ions in soils and groundwaters. A thorough understanding of the structural environment of metals at the solid−water interface is therefore of fundamental importance. In this study, X-ray absorption fine structure (XAFS) spectroscopy was used to discern the local atomic structure of Ni(II) sorbed onto pyrophyllite. The first coordination shell consists of 6 O atoms at 2.02−2.04 Å. For the second shell, XAFS data suggest a single Ni−Al/Si distance (2.96−3.03 Å), indicative of edge sharing of Ni and Al octahedra and possibly the presence of mixed nickel−aluminum hydroxides. As Ni surface loading on pyrophyllite increased, the number of Ni second-neighbor atoms at a distance of 2.99−3.00 Å increased from $N \approx 1$ to $N \approx 5$. The presence of multinuclear surface complexes was depicted at low surface loading and at reaction conditions undersaturated with respect to the formation of $Ni(OH)_2$(s). This observation suggests that the total coverage of surface sites is not necessary for the formation of multinuclear surface complexes and implies that the pyrophyllite surface promotes hydrolysis and multinuclear complex formation.

Introduction

Accumulation of excessive amounts of trace elements such as nickel in soils can have a toxic effect on soil organisms and plants. Natural soil concentrations of total Ni are normally <2 mmol kg^{-1} (*1*). Anthropogenic input (e.g., from tanneries, smelters, or sewage sludge application), however, can increase the total Ni concentration in soils to >50 mmol kg^{-1} (*2*), which may be toxic to plants (*1*).

In soils, Ni exists in various solid and solution forms. In solution, the free aqua ion (Ni^{2+}) is normally the predominant species, but Ni can also form complexes with various inorganic and organic ligands (*2*). In the solid phase, Ni is found in various mineral forms (*3, 4*). One of the most important aspects of Ni interaction in soils, however, is sorption on mineral surfaces.

* Corresponding author telephone: 302-831-1595; fax: 302-831-3651; e-mail address: scheideg@brahms.udel.edu.

† University of Delaware.

‡ Brookhaven National Laboratory.

Adsorption of Ni on clay minerals has been extensively studied (*2, 5−9*). Nickel adsorption onto kaolinites decreased with increasing ionic strength, and greater adsorption occurred on Na- than on Ca-saturated clays (*2*). When sulfate was the dominant solution anion, adsorption of Ni was depressed relative to that obtained with nitrate due to Ni−sulfate complexation. The exchange reactions of K−Ni and Ca−Ni on kaolinite were nonideal (*6*). A stronger binding of Ni on the kaolinite surface was suggested by the negative enthalpy changes. The selectivity sequence for the adsorption of Cd, Ni, and Zn on kaolinite was Cd > Zn > Ni and on montmorillonite was Cd ≈ Zn > Ni (*8*). Schulthess and Huang (*9*) explained the adsorption of Ni onto kaolinite by a combination of the adsorption behavior of Ni onto silicon and aluminum oxide surfaces.

Over the past several decades, surface complexation models have been developed and applied to describe metal sorption reactions at the solid−water interface (*10−12*). These models have been used to mechanistically interpret the sorption reactions. Surface complexation models are predominantly based on the conception that metal ions form complexes with surface functional groups in a manner similar to metal−ligand associations in the solution phase. A surface complexation model was used to describe the adsorption of Cu, Cd, and Pb on kaolinite (*13*). This model consisted of two types of adsorption sites: (a) weakly acidic sites capable of forming outer-sphere complexes and (b) ampholytic surface hydroxyls (AlOH) responsible for chemical bonding of the metal ions to the kaolinite surface by formation of inner-sphere complexes.

Only a few models have considered surface precipitation reactions (*14−16*). In surface precipitation, cations that adsorb to the surface of a mineral form at high surface coverage a precipitate of the cation with the constituent ions of the mineral (*17*). A model has been proposed (*15*) that allows for a continuum between surface complex formation and bulk precipitation of the sorbing ion; i.e., as the cation is complexed at the surface, a new hydroxide surface is formed. In this model, cations at the solid−water interface are treated as surface species while those not in contact with the solution phase are treated as solid species forming a solid solution (*15, 17*).

Surface complexation models, however, are not unique descriptions. They are often based on macroscopic data and cannot be used to infer sorption mechanisms and to distinguish adsorption from surface precipitation without direct molecular-level evidence (*18*). Surface spectroscopy offers the best hope for a molecular-level probe of the interfacial region because it provides structural and chemical information about surface complexes (*19−21*). One should recognize, however, that most surface spectroscopic methods probe the average state of an element in a sample and are therefore not strictly molecular.

Recent studies using surface analytical methods have demonstrated that the adsorption of heavy metals on clay and oxide surfaces results in the formation of multinuclear or polynuclear surface complexes much more frequently than previously thought. Multinuclear metal hydroxides of Pb, Co, Cu, and Cr(III) on oxides and aluminosilicates have been discerned with XAFS (*22−27*) and electron spin resonance (ESR) spectroscopy (*28−30*). Such surface

0013-936X/96/0930-0548$12.00/0

complexes, or surface precipitates, have been observed at metal surface loadings far below a theoretical monolayer coverage and in a pH range well below the pH where the formation of metal hydroxide precipitates would be expected according to the thermodynamic solubility product (*25*−*27*).

In this study, XAFS spectroscopy was used to determine the local structural environment of Ni(II) sorbed onto pyrophyllite. Spectroscopic data were collected in situ, i.e., an aqueous Ni solution in contact with the pyrophyllite surface. Changes in the XAFS spectra with increasing Ni uptake were examined. Short-term and long-term equilibrated samples were compared and correlated to dissolved Si and Al concentrations.

Pyrophyllite was chosen for these experiments in order to study the effect of edge surface properties of clays on Ni sorption. Pyrophyllite, in contrast to montmorillonite and illite, shows little deviation from the ideal chemical formula ($Al_2Si_4O_{10}(OH)_2$) of 2:1 clays. A very small substitution of Al for Si can occur which is commonly ~0.001 Al cations per formula unit (*31*). Its dioctahedral structure consists of essentially neutral tetrahedral−octahedral−tetrahedral layers. Hence, the complexity associated with the permanent charge of planar clay surfaces can be avoided and sorption of ions on pyrophyllite can be ascribed to only edge surface sites (*32*).

Experimental Section

Materials. Pyrophyllite [$Al_2Si_4O_{10}(OH)_2$] used in this study originated from North Carolina (Ward Natural Science, 46E4630). The pyrophyllite was ground in a mortar to a size fraction of $<125\ \mu$m and transferred to a porcelain ball mill which was one-third filled with hard ball-shaped, wear-resistant media (zirconia). The pyrophyllite was then ground dry for 30 h. The $<2\ \mu$m clay fraction was obtained by centrifuging and decanting. The clay was saturated with Na by washing three times with 0.5 M $NaNO_3$. The clay was resuspended with distilled water and centrifuged. The clear supernatant was discarded, and excess salts were removed by dialysis until the electrical conductivity of the equilibrium solution was $<10\ \mu S\ cm^{-1}$. Thereafter, the white clay material was freeze-dried.

Pyrophyllite was characterized by X-ray diffraction (XRD; Philips, PW1729) and diffuse reflectance infrared Fourier transform spectroscopy (DRIFT; Perkin-Elmer 1720X spectrometer). The IR spectra showed only characteristic peaks for pyrophyllite (*33*), while XRD spectra suggested the presence of a small amount of quartz (<5%) in addition to pyrophyllite. No porcelain or zirconia residuals from the grinding process could be detected. The specific surface area of pyrophyllite was determined by the BET method using N_2 adsorption and the ethylene glycol monoethyl ether (EGME) method (*34*). The variation between these two methods was small (BET = 96.3 $m^2\ g^{-1}$; EGME = 95 $m^2\ g^{-1}$), which demonstrates that no significant amount of swelling clay, such as montmorillonite, was present in the pyrophyllite. In this paper, we will use the BET specific surface area value.

Batch Studies. Samples for XAFS analysis were prepared using a batch technique designed to maintain constant pH (pH-stat, Radiometer) and temperature (298 K) and to eliminate CO_2 by purging with N_2. Pyrophyllite was hydrated in a 0.1 M $NaNO_3$ solution for 24 h prior to reaction with Ni. After hydration the pH of the suspension was adjusted to pH = 7.5 with 0.1 M NaOH, and the mixture was brought to a solid/liquid ratio of 20 g/L. A desired amount of Ni from a 0.1 M $Ni(NO_3)_2$ stock solution (pH ≈ 6) was dispensed in stepwise additions within a 15 min period into a large batch reaction vessel (800 mL) to avoid the formation of Ni precipitates due to local oversaturation of the suspension. The pH was automatically held constant (pH = 7.5). After a reaction time of 24−48 h a 40 mL suspension was removed and placed in a vial, and further small Ni increments were added to the main reaction vessel. The above procedure was repeated for each sample. The collected samples were immediately centrifuged, and the supernatant was passed through a $0.22\ \mu$m membrane filter. The clear solutions were then analyzed by inductively coupled plasma emission (ICP) spectrometry. The remaining wet pastes were washed with 50 mL of high-purity water to adequately remove entrained electrolyte and then centrifuged again. The washing process was repeated twice and resulted in no significant Ni desorption. The samples were then sealed and stored in a refrigerator to keep them moist for XAFS analysis.

Initial Ni concentrations (0.6−4 mM) and the reaction pH (pH = 7.5) were selected to achieve >90% Ni removal from solution, resulting in sorption densities, Γ, of 0.27−2.0 μmol m^{-2} (based on the total surface area of the clay). All samples were unsaturated with respect to $Ni(OH)_2$. The sorption data gleaned with this method are representative of the reaction after a 24−48 h time period and, therefore, may not be indicative of sorption at equilibrium. These samples will be called short-term equilibrated samples.

The kinetics of Ni sorption from a 3 mM solution was measured at a constant pH (pH = 7.5) and an ionic strength of 0.1 M ($NaNO_3$). The solid/liquid ratio for this experiment was 10 g/L. Samples were passed through a $0.22\ \mu$m pore membrane and analyzed by ICP for Ni, Al, and Si. After a reaction time of ~200 h, the Ni-treated pyrophyllite suspension was centrifuged. The wet paste was then washed to remove entrained electrolyte and stored as before. This XAFS sample will be called the long-term equilibrated sample.

The dissolution rate of pyrophyllite at pH = 7.5 was determined using the pH-stat apparatus. Samples were collected at regular time intervals and the filtered solutions analyzed for Al and Si as before.

XAFS Studies. XAFS spectra were recorded at beamline X-11A at the National Synchrotron Light Source, Brookhaven National Laboratory, Upton, NY. The electron storage ring operated at 2.528 GeV with an average current of 180 mA. A Si (111) crystal was employed in the monochromator with a sagittally focused beam (*35*). The focused beam increased the flux intensity over the investigated energy range by roughly a factor of 3 relative to a normal flat monochromator arrangement. A 0.5 mm premonochromator slit width was employed. The height of the entrance slit was readjusted as necessary to compensate for vertical motion of the stored electron beam. Higher-order harmonic rejection was achieved by detuning slightly the angle of one monochromator crystal with respect to the other until the harmonic contribution was negligible.

Beam energy was calibrated by assigning the first inflection on the K-absorption edge of a nickel metal foil to an energy of 8333 eV. The spectra were collected in fluorescence mode using a Stern−Heald-type detector (*36*) which is available commercially (The EXAFS Co.) and known as a Lytle detector (*37*). The samples were placed at a 45° angle to the incident beam, and a wide-angle collector with

the ionization chamber was located 45° off the sample. The Lytle detector was filled with krypton, and the gas was replenished every 3 h. A Co filter and Soller slits were placed between the sample and the detector to reduce elastically scattered X-rays from entering the fluorescence detector. The spectra were run at 77 K to reduce damping of the XAFS oscillation by thermal disorder. Comparisons of spectra recorded at 77 K and room temperature revealed no change in structural information while the signal-to-noise ratio was maximized by lowering the temperature (*22*, *25*).

Ni-bearing pyrophyllite samples were packed into a 4 × 6 × 25 mm slot cut in a stainless steel block. The dimension of the slot cut provided 1 mm on each side of the beam and a depth in excess of four absorption lengths when mounted at 45° to the incident beam. The samples were sealed with a 0.0005 in. thick Kapton ploymide tape (CHR Industries, type K-104) to avoid moisture loss while minimizing X-ray absorption. The samples were then mounted on a Cu cold finger that was connected to a liquid N_2 reservoir. To eliminate the possibility of a XAFS contribution from Ni impurities in the stainless steel block, the whole setup was covered with a Pb foil. To minimize the heat transfer imposed on the cold finger, samples were precooled by immersion into N_2(l) for several minutes prior to analysis. All scans were collected at least in triplicate and averaged to improve the signal to noise ratio.

Data Analysis. Data analysis was accomplished using the program EXCURV90 (*38*). The background of the spectra was subtracted using a cubic spline fit technique. After normalization, the raw absorption data were converted from energy to k space and weighted by k^2 in order to compensate for the damping of the XAFS amplitude with increasing k. The zero energy point, E_o, was taken as the edge inflection point and was treated as an adjustable fitting parameter. Amplitude parameters and phase shifts for Ni, O, and Si were obtained experimentally from the spectra of crystalline $Ni(OH)_2$ and NiSi. For XAFS data collection, the reference compounds were lightly crushed to powders with an agate mortar and pestle and diluted with boron nitride.

Successive shells were isolated in the Fourier-transformed spectra, back-transformed, and fitted in k space by adjustment of the zero energy point E_o, the interatomic distances (Rs), coordination number (Ns), and Debye–Waller-type terms until a best fit was obtained between the predicted and experimental curves. Fitting was done using data in the k range 3.4–14.2 $Å^{-1}$. The obtained structural parameters for each shell were then combined to model the entire spectrum using a multishell fit and components out to 3.9 Å.

Errors given were estimated on the basis of the fitting results. The R values were accurate to ±0.02 Å, and the N values were accurate to ±20% for the first shell and ±40% for the second shell.

Results

Figure 1 illustrates the kinetics of Ni sorption on pyrophyllite from a 3 mM Ni solution at pH = 7.5 and of dissolved Si from Ni-treated and Ni-untreated pyrophyllite. Si data were corrected for the small Si concentrations (~1×10^{-4} M) present in solution at the beginning of the experiments due to the preceding hydration process of the clay. A sample that had been reacted with Ni for ~200 h was used for XAFS measurements (long-term equilibrated sample). Figure 1 shows that Ni sorption was initially rapid and then decreased gradually. After 72 h, Ni sorption was nearly complete (97% of the initial Ni was sorbed). The Si concentration, at any moment during Ni sorption, was at least 10 times smaller than the initial Ni concentration. The dissolution of pyrophyllite seemed to be influenced by Ni sorption since the initial dissolution rate was enhanced compared to the dissolution rate of pyrophyllite without Ni (Figure 1). The latter dissolution rate during the experiment was 3.2×10^{-13} mol m^{-2} s^{-1} (pH = 7.5, time range 0–216 h) which was comparable to a dissolution rate of 2.5×10^{-13} mol m^{-2} s^{-1} for kaolinite at pH = 6.5 (*39*). However, the dissolution rate of pyrophyllite was significantly smaller than the dissolution rate of silica [1×10^{-11} mol m^{-2} s^{-1} at pH = 7.5 (*40*)].

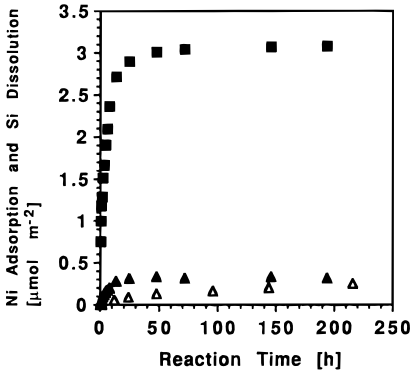

FIGURE 1. Kinetics of Ni sorption on pyrophyllite from a 3×10^{-3} M Ni solution at pH = 7.5. (■) denotes the amount of sorbed Ni (μmol m^{-2}) and (▲) the amount of simultaneous dissolved Si (μmol m^{-2}). The dissolution of untreated pyrophyllite at pH = 7.5 is shown for comparison (△).

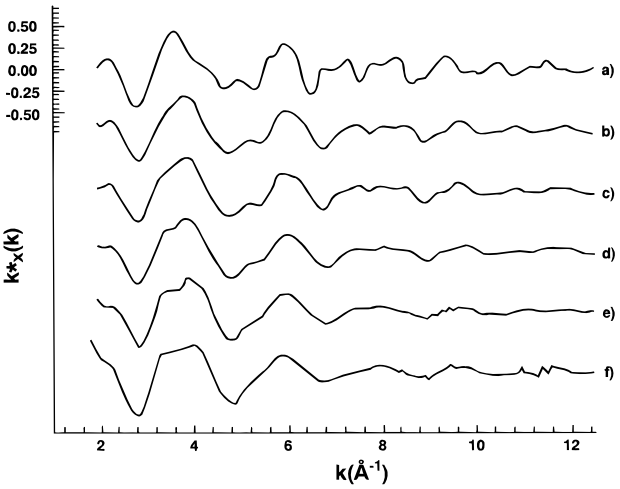

FIGURE 2. *k*-weighted, normalized, background-subtracted XAFS spectra of Ni sorbed on pyrophyllite at surface sorption densities, Γ, of (b) 3.1, (c) 2.0, (d) 1.0, (e) 0.49, and (f) 0.27 μmol m^{-2} compared to the spectrum of the crystalline $Ni(OH)_2$(s) model compound (a).

Figure 2 shows normalized, background-subtracted and k-weighted XAFS spectra of Ni sorbed on pyrophyllite. The surface sorption densities varied from Γ = 0.27–3.1 μmol m^{-2}. The spectrum of the reference compound, crystalline $Ni(OH)_2$, is shown for comparison. At high Ni sorption density, for example, Γ = 3.1 μmol m^{-2}, a complicated "beat" pattern is evident in the XAFS spectra which indicates the presence of backscattering atoms beyond the first coordination shell.

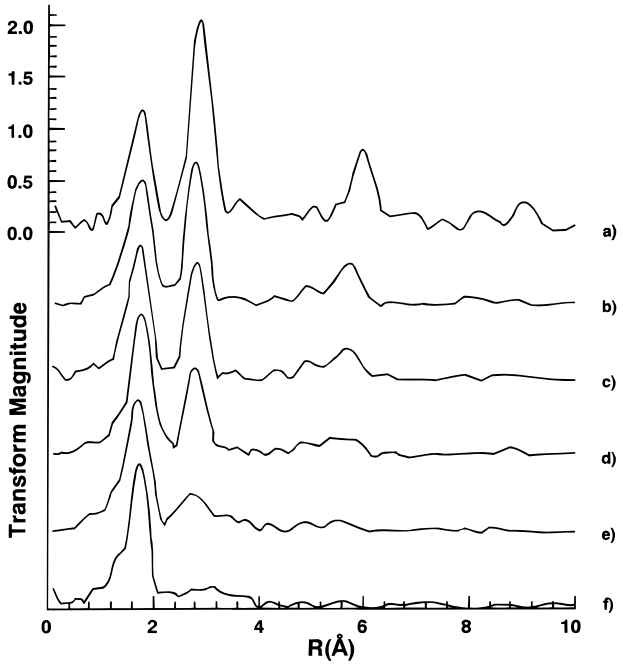

FIGURE 3. Radial structure functions (RSFs) Ni-treated pyrophyllite samples at surface sorption densities, Γ, of (b) 3.1, (c) 2.0, (d) 1.0, (e) 0.49, and (f) 0.27 μmol m^{-2} compared to the spectrum of the crystalline $Ni(OH)_2$(s) model compound (a). The spectra are uncorrected for phase shift. Note the appearance of a peak at a *R* of about 2.7 Å with increasing sorption density.

Figure 3 illustrates radial structure functions (RSFs) produced by Fourier forward transforms of the spectra represented in Figure 2. The spectra were uncorrected for phase shift. Fourier transform of Ni-treated pyrophyllite spectra indicated changes in absorber−backscatterer correlation that changed with increasing surface coverage. At the lowest Ni uptake (Γ = 0.27 μmol m^{-2}; Figure 3f), the peak at $R \sim 1.7$ Å which represents the first shell is dominant, while peaks beyond are small. With increasing surface loading (Γ = 0.51−3.1 μmol m^{-2}), the peak at $R \sim 2.7$ Å, which represents the second shell, increased in intensity with increasing Ni uptake (Figure 3b−e). The spectrum of $Ni(OH)_2$(s) (Figure 3a) showed a similar peak at a slightly higher *R*. There was also a peak beyond the second shell at $R \sim 5.8$ Å and at higher surface loadings (Figure 3b,c). This peak, also present in the $Ni(OH)_2$ reference spectrum, resulted from multiple scattering among Ni atoms (*27*) and will not be discussed further.

The structural parameters derived from XAFS analysis are summarized in Table 1. Least-squares fits of filtered XAFS of the first RSF peak indicate ~6 O atoms at 2.02−2.04 Å, independent of the Ni sorption density. The solution for the fit of the second shell is mathematically not unique. Best fits were obtained by incorporating Ni and Si or Al as second-neighbor backscatterer atoms. Because Si and Al differ in atomic number by 1 (*Z* = 13 and 14, respectively), backscattering is similar. They cannot be easily distinguished from each other as second-neighbor backscatterers, especially in circumstances such as this where the contribution of both is small and cannot be resolved from another in the Fourier transform.

Table 1 reveals that as the Ni surface loading on pyrophyllite increases from Γ = 0.27 to 3.1 μmol m^{-2}, the number of Ni second-neighbor (*N*) atoms at a distance of 2.99−3.00 Å increases from *N* = 0.8 to 4.8, indicating the

TABLE 1

Structural Information Derived from XAFS Analysis Using EXCURV90: Interatomic Distances (*R*, Å), Coordination Numbers (*N*), and Debye−Waller factors ($2\sigma^2$, Å^2)[a]

		Ni−O			Ni−Ni			Ni−Si/Al		
Γ (μmol m^{-2})	ΔE_0 (eV)	*R* (Å)	*N*	$2\sigma^2$	*R* (Å)	*N*	$2\sigma^2$	*R* (Å)	*N*	$2\sigma^2$
$Ni(OH)_2$	0.0	2.06	6.0	0.011	3.09	6.0	0.010			
3.1	3.3	2.02	6.1	0.010	3.00	4.8	0.009	3.02	2.7	0.009
2.0	3.2	2.03	6.1	0.009	3.00	3.4	0.008	3.03	1.8	0.010
1.0	1.6	2.03	5.7	0.007	3.00	3.0	0.009	3.01	2.1	0.009
0.49	1.5	2.03	6.6	0.011	2.99	1.6	0.010	2.96	1.5	0.010
0.27	−3.0	2.04	5.7	0.010	3.00	0.8	0.011	2.96	1.2	0.009

[a] The reported values are accurate to within $R \pm 0.02$ Å, $N_{(Ni-O)} \pm 20\%$, $N_{(Ni-Ni)} \pm 40\%$, $N_{(Ni-Si/Al)} \pm 40\%$. ΔE_0 (eV) represents the threshold energy and is the difference between E_0 in reference and sample spectra.

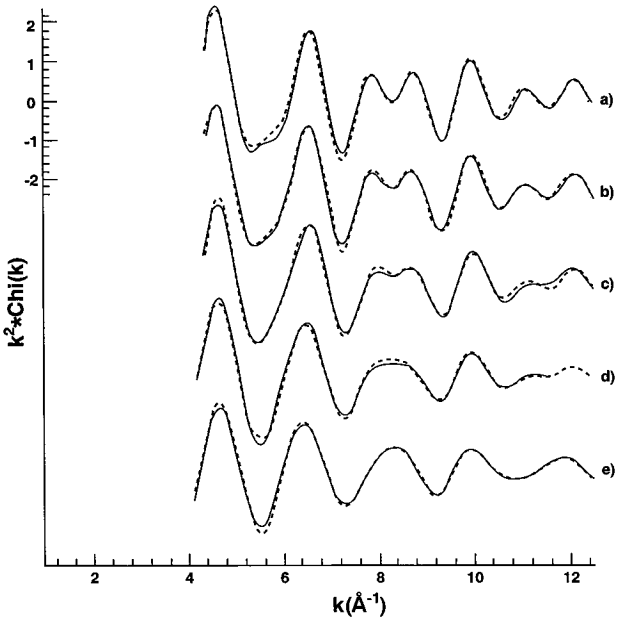

FIGURE 4. k^2-weighted XAFS functions (solid line) for the Fourier-back-transformed spectra at surface sorption densities, Γ, of (a) 3.1, (b) 2.0, (c) 1.0, (d) 0.49, and (e) 0.27 μmol m^{-2}. The theoretical spectra were derived with parameters from analysis of the isolated shells (dashed line).

formation of multinuclear complexes with increasing numbers of Ni atoms. Compared to crystalline $Ni(OH)_2$(s), Ni−Ni distances are however shortened ~0.1 Å. In $Ni(OH)_2$(s), Ni−Ni distances are 3.09 Å and agree with values from the literature (*4*, *41*, *42*). At the lowest Ni uptake (Γ = 0.27 μmol m^{-2}), second-neighbor backscattering from Ni is small (*N* = 0.8) and second-neighbor backscattering can possibly be attributed to only Si/Al atoms. XAFS data suggest the presence of approximately one to two second-neighbor atoms at 2.96 Å. With increasing Ni sorption density, the number of second-neighbor backscattering atoms from Si or Al remains more or less constant ($N_{Ni-Si/Al}$ between 1.5 and 2.1). The corresponding distances increase slightly (2.96−3.03 Å). At the highest surface loading (Γ = 3.1 μmol m^{-2}), $N_{Ni-Si/Al}$ seems to be insignificantly enhanced ($N_{Ni-Si/Al} = 2.7$).

Figure 4 shows a comparison of k^2-weighted XAFS functions for the Fourier-back-transformed spectra to the theoretical spectra derived with parameters from analysis of the isolated shells. One can observe a good agreement

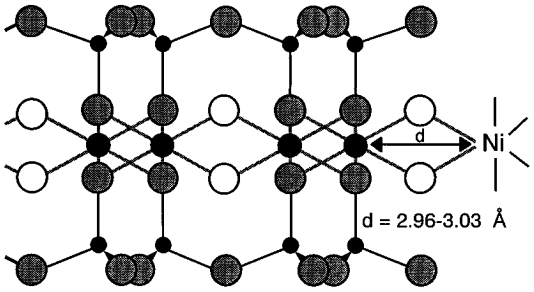

FIGURE 5. Proposed edge site morphology for pyrophyllite adapted from White and Zelazny (*47*). Shaded circles denote oxygen atoms, open circles are hydroxyls, the small filled circles are silica atoms, and the larger filled circles are aluminum atoms. Edge sharing between Ni and the Al octahedron results in a single Ni−Al distance (2.96−3.03 Å) representing a possible mode for attachment of Ni to the pyrophyllite surface.

between the Fourier-back-transformed XAFS function and the theoretical fit over the whole energy range (up to 12 K).

Discussion

Binding of Ni on Pyrophyllite. XAFS analysis suggested that in the first coordination shell Ni is surrounded by 6 O atoms. This behavior indicated that Ni(II) is in an octahedral environment. The Ni−O bond distance and coordination numbers were not affected by the Ni sorption density. For the second coordination sphere, the data suggested the presence of multinuclear surface complexes. Additionally a Ni−Si/Al distance between 2.96 and 3.03 Å is observed. Given the octahedral coordination of Ni, a distance of 2.96−3.03 Å is too long for tridentate bonding (<2.4 Å) and too short for monodentate bonding (>3.2 Å). Bonding of a hydrated Ni ion to the pyrophyllite surface by outer-sphere complexation would result in Ni−Al/Si distances of >5 Å. Thus, the data indicate that Ni binds to pyrophyllite as a bidentate inner-sphere surface complex.

In the following discussion, we use a polyhedral approach (*21*, *43*−*45*) to discuss how Ni might be bound to the pyrophyllite surface. This approach assumes that pyrophyllite serves as a substrate and that Ni bonds to the surface as a regular, oxygen-coordinated octahedron with a minimum amount of distortion. Possible modes of attachment of Ni to the pyrophyllite surface can be deduced by comparing O−O distances in Ni octahedra with O−O distances in Si and Al polyhedra in pyrophyllite.

Edge O−O distances in Ni octahedra derived from XAFS measure 2.86−2.88 Å, assuming a regular octahedron. Bond distances in pyrophyllite calculated from XRD measurements (*46*) show that O−O distances vary over a significant range. O−O distances in Si tetrahedra range from 2.61 to 2.66 Å (mean, 2.64 Å). O−O distances in Al octahedra vary from 2.76 to 2.93 Å (mean, 2.81 Å). Edge sharing between a Ni octahedron and a Si tetrahedron is unlikely due to the large differences in O−O distances. Edge sharing between a Ni octahedron and a distorted Al octahedron represents a possibility since O−O distances of Ni and Al octahedra overlap.

Figure 5 illustrates edge sharing of Ni and Al octahedra as a plausible mode of attachment of Ni to the pyrophyllite surface. Edge sharing of Ni and Al octahedra can explain why we observed a single Ni−Al/Si distance (2.96−3.03 Å) and would be consistent with the fact that nonbridging Al−OH sites along the particle edge are considered to be the most reactive sites for pyrophyllite in a common environmental pH range (pH = 3−9) (*47*). On the other hand, we cannot explain the number of Ni second-neighbor backscatter atoms by edge sharing of Ni and Al octahedra alone. With increasing Ni uptake, N_{Ni-Ni} increases from about 1 to 5, while $N_{Ni-Si/Al}$ seems to be hardly affected by the increasing sorption density (see Table 1). One would expect that $N_{Ni-Si/Al}$ decreases relative to the increasing N_{Ni-Ni}, since an increased N_{Ni-Ni} indicates the formation of multinuclear complexes with increasing numbers of Ni atoms.

The formation of mixed nickel−aluminum hydroxides may explain the observed bond distances and coordination numbers. The existence of mixed-cation hydroxide phases has been reported in the literature (*48*−*50*). These compounds consist of pyroaurite-like structures in which divalent and trivalent metal ions are randomly distributed within the same octahedral hydroxide sheet. Anions such as Cl^-, Br^-, I^-, NO_3^-, OH^-, and CO_3^{2-} can occupy the region between the hydroxide sheets. The synthesis of mixed-cation hydroxide compounds can be performed by precipitation of one cation [e.g., Al(III)] as a hydroxide from solution with the pH of the suspension maintained just below the value at which the second cation hydroxide [e.g., $Ni(OH)_2$] would precipitate (*50*). In mixed nickel−aluminum hydroxides the Ni/Al cation mole ratio can vary between 1.3 and 4.8 (*49*, *50*). Ni−Ni distances in these compounds are 3.05 Å (*47*, *48*) and therefore distinctly shorter than those in $Ni(OH)_2$.

We could not detect dissolved Al in our samples. Even so, Al could have been released into solution and incorporated into mixed nickel−aluminum hydroxides. The amount of released Al can be estimated based on the chemical composition of pyrophyllite [$Al_2Si_4O_{10}(OH)_2$] and the dissolution rate of the clay at pH = 7.5 (see Results section). Assuming stoichiometric dissolution, the amount of released Al for the long-term equilibrated sample is ~20 times smaller than the amount of sorbed Ni. For this reason we think that the formation of mixed nickel−aluminum hydroxides represents a possible but not the most dominant sorption mode of Ni in our experiments.

Furthermore, if a significant amount of Ni would form mixed nickel−aluminum hydroxides, one would expect this reaction to affect the structural environment of Ni in the long-term spectrum. Indeed, we observe that second-neighbor backscattering from Si or Al is insignificantly increased in the long-term equilibrated sample ($N_{Ni-Si/Al}$ = 2.7) relative to the short-term equilibrated samples ($N_{Ni-Si/Al}$ = 1.2−2.1). The bond distances and Debye−Waller factors that account for thermal and static disorder however are very similar, with respect to Ni−Ni as well Ni−Si/Al backscattering. Unfortunately, the long-term sample also had the highest Ni concentration, which makes it difficult to understand the effect of reaction time on the structural environment of Ni.

It would be useful to compare our findings with the XAFS results of Co sorption on kaolinite (*26*, *27*). With increasing surface coverage the number of second-neighbor Co atoms increased from about 2 to 6. Co−Co distances (R = 3.10−3.12 Å) were 0.05−0.07 Å shorter compared to crystalline $Co(OH)_2$, and a single Co−Al/Si distance (R = 3.14−3.15 Å; $N_{Co-Si/Al}$ = 0.7−1.4) was detected which could be attributed to edge sharing between Co and Al octahedra on either edge or on the (001) faces of kaolinite. The results of our study and the Co−kaolinite studies are very similar. They differ only insofar as that in one Co study (*26*) two distinct Co−Al/Si distances (~2.7 and ~3.4 Å) were observed

at low Co sorption densities. The authors proposed corner-sharing between two bridging Al−O−Si sites or one bridging Al−O−Si and one Al−OH inner-hydroxyl site (*26*). Charlet and Manceau (*21*, *51*) argued, however, that the combination of a M−M [e.g., M = Co(II), Ni(II), Mg(II)] distance between 3.0 and 3.12 Å and the presence of a Si/Al shell near 3.22−3.29 Å is only achieved in a trioctahedral clay-like structure. The specific feature of this configuration is shortening M−M distances across edges compared to those in the $M(OH)_2$ structure. For instance, the Ni−Ni distance is equal to 3.0 Å in Ni talc and 3.09 Å in $Ni(OH)_2$ (*4*). Multinuclear surface complexes or surface precipitates formed by the sorption of Co and Ni onto silicate surfaces were interpreted as neoformed hydrous silicates which result from a precipitation process (*21*, *51*).

In our case, we doubt that the so-called neoformation of clays is responsible for the observed backscattering pattern for the following reasons: (a) The data show no indication of a shell between or near 3.2−3.3 Å and suggest instead a single Ni−Al/Si distance (2.96−3.03 Å), (b) the amount of dissolved Si during the experiment is much smaller than the amount of sorbed Ni, and (c) in case a significant amount of Ni would form clay-like structures with silicates, one would expect to see a decrease in the dissolution rate. However, our data suggest an increase. It seems that surface complexes of Ni on pyrophyllite destabilize surface metal ions (Al and Si) relative to the bulk solution and, therefore, lead to an enhanced dissolution of the clay. This would explain why the enhanced dissolution rate is only observable where Ni sorption is pronounced (see Figure 1).

XAFS data suggested bidentate inner-sphere Ni complexation via edge sharing of Ni and Al octahedra as one plausible mode of attachment and the formation of mixed nickel−aluminum hydroxides as another. To definitively ascertain the sorption mechanism, other surface analysis techniques such as high resolution transmission electron microscopy and atomic force microscopy, in addition to XAFS, could be employed to gain detailed atomic and morphological information about the nature of the multinuclear Ni complexes on the pyrophyllite surface.

From Adsorption to Surface Polymerization and Precipitation. In solution, nucleation is restricted to supersaturated systems. Several studies using surface spectroscopic methods such as XAFS, ESR, and XPS provide evidence that the multinuclear surface complexes persist in systems undersaturated with respect to homogeneous precipitation (*22*, *25*−*30*, *52*). We observe the formation of surface species containing Ni clusters from solutions that are undersaturated with respect to the thermodynamic solubility product of $Ni(OH)_2(s)$. Figure 6 shows the calculated concentrations of Ni species in homogeneous solution when $[Ni] = 1 \times 10^{-3}$ M and the ionic strength, $I = 0.1$ M. Nickel is predominately present as $Ni^{2+}(aq)$ and to a minor extent as $Ni(NO_3)^-(aq)$. The concentrations of hydrolysis products such as $Ni(OH)^+$ and $Ni(OH)^{3-}$ are extremely low. This finding implies that the pyrophyllite surface promotes hydrolysis and/or stabilizes multinuclear surface complexes.

Oversaturation with respect to the surface sites (which occurs whenever the sorbate surface excess becomes larger than the density of the surface site) may result in the formation of multinuclear surface complexes. Recent XAFS studies reveal that nucleation processes can also occur in systems undersaturated with respect to the surface sites.

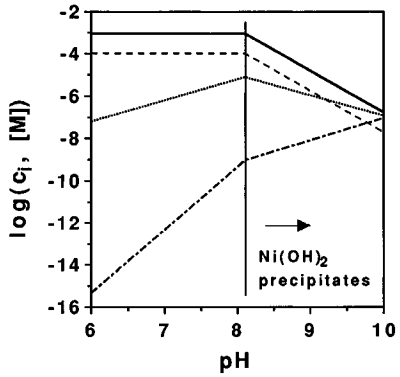

FIGURE 6. Solution speciation for 1×10^{-3} M Ni in aqueous solution (0.1 M $NaNO_3$) as predicted by a chemical equilibrium speciation program based on a thermodynamic database (Environmental Simulation Program, OLI Systems, Morristown, NJ). Data reported in refs 55−59 were considered. The solid line denotes the concentration (log c_i [M]) of Ni^{2+}, the dashed line the concentration of $Ni(NO_3)^-$, the dotted line the concentration of $Ni(OH)^+$, and the dashed dotted line the concentration of $Ni(OH)_3^-$. The vertical line in the figure represents the pH where the formation of nickel hydroxide precipitates in homogeneous solution is expected.

For Co(II) sorption on kaolinite (*26*, *27*), TiO_2, and γ-Al_2O_3 (*23*), XAFS data indicate the formation of multinuclear surface complexes at surface coverages corresponding to <5% of a monolayer of oxygen-bound Co atoms averaged over the BET surface area. Nucleation processes of Cr(III) on hydrous ferric oxide were observed at site occupancies of <10% (*22*) and on a silica surface at site occupancies of 20% (*25*). Our XAFS data also suggest the presence of multinuclear complexes at low sorption densities; e.g., $\Gamma = 0.49$ μmol m^{-2}. If the closest packing of NiO_6 polyhedra is assumed to constitute a monolayer of Ni atoms, $\Gamma = 0.49$ μmol m^{-2} corresponds to <5% of monolayer coverage. If surface density is based on the surface of edge sites only it represents ~25% occupancy [assuming that the pyrophyllite particles have a square planar surface shape with a size of 2 μm and a thickness of 0.25 μm (*32*)]. White and Zelazny (*47*) calculated the concentration of edge-charge sites on pyrophyllite and determined a site density of 7.0 μmol m^{-2} for octahedral nonbridging Al−OH sites. If one assumes that Ni sorbs as a bidentate complex on these sites only, a sorption density of 0.49 μmol m^{-2} represents ~14% occupancy.

An approximate estimate of the number of sites can also be obtained by employing different experimental methods. The maximum proton release at high pH values may be taken as an estimate of the concentration of ionizable groups. Acid−base titration data for pyrophyllite (*53*) suggest a site density of 4.8 μmol m^{-2} and a site occupancy of <20%, assuming that Ni sorbs as a bidentate complex.

The number of surface sites is a nebulous parameter that is methodology-dependent. The estimated site density obtained from different methods is typically different by a factor of 2−3 and sometimes more (*54*). In spite of the uncertainty in determining the number of sites, our XAFS data show the presence of multinuclear Ni complexes at sorption densities which seem to be well below monolayer coverage. This observation suggests that the total coverage of surface sites is not responsible for the formation of multinuclear nickel complexes on the pyrophyllite surface.

Acknowledgments

We thank M. J. Kelley (DuPont Co.) for performing the BET surface area measurements, J. Wallach (National Institute of Standards and Technology, Gaithersburg, MD) for grinding the pyrophyllite, Cathy Olsen for the ICP measurements, and Tim Alcacio for the careful reading of the manuscript. We gratefully acknowledge the support of this research by the DuPont Co.

Literature Cited

(1) Adriano, D. C. *Trace Elements in the Terrestrial Environment*; Springer: Berlin, 1986; pp 362−389.
(2) Mattigod, S. H.; Gibali, A. S; Page, A. L. *Clays Clay Miner.* **1979**, *27*, 411.
(3) Manceau, A.; Calas, G. *Am. Mineral.* **1985**, *70*, 549.
(4) Manceau, A.; Calas, G. *Clay Miner.* **1986**, *21*, 341.
(5) Koppelmann, M. H.; Dillard, J. G. *Clays Clay Miner.* **1977**, *25*, 457.
(6) Bansal, O. P. *J. Soil Sci.* **1982**, *33*, 63.
(7) Tiller, K. G.; Gerth. J.; Brümmer, G. *Geoderma* **1984**, *34*, 17.
(8) Puls, R. W.; Bohn, H. L. *Soil Sci. Soc. Am. J.* **1988**, *52*, 1289.
(9) Schulthess, C. P.; Huang, C. P. *Soil Sci. Soc. Am. J.* **1990**, *54*, 679.
(10) Benjamin, M. M.; Leckie, J. O. *J. Colloid Interface Sci.* **1981**, *79*, 209.
(11) Schindler, P. W.; Stumm W. In *Aquatic Surface Chemistry*; Stumm, W., Ed., Wiley and Sons: New York, 1987; pp 83−110.
(12) Hiemstra, T; De Wit, J. C. M.; Van Riemsdijk, W. H. *J. Colloid Interface Sci.* **1989**, *133*, 91.
(13) Schindler, P. W.; Liechti, P.; Westall, J. C. *Neth. J. Agric. Sci.* **1987**, *35*, 219.
(14) James, R. O.; Healy, T. W. *J. Colloid Interface Sci.* **1972**, *40*, 53.
(15) Farley, K. L.; Dzombak, D. A.; Morel, F. M. M. *J. Colloid Interface Sci.* **1985**, *106*, 226.
(16) Katz, L. K. Ph.D. Thesis, University of Michigan, Ann Arbor, MI, 1993.
(17) Stumm, W. In *Chemistry of the Solid−Water Interface*; Stumm, W., Ed., Wiley and Sons: New York, 1992; p 229.
(18) Sposito, G. In *Geochemical Processes at Mineral Surfaces*; Davis, J. A., Hayes, K. F., Eds.; ACS Symposium Series 323: American Chemical Society: Washington, DC, 1986; pp 217−228.
(19) Motschi, H. In *Aquatic Surface Chemistry*; Stumm, W., Ed.; Wiley and Sons: New York, 1987; pp 11−125.
(20) Brown Jr., G. E. *Rev. Mineral.* **1990**, *23*, 309.
(21) Charlet L.; Manceau, A. In *Environmental Particles*; Buffle, J., van Leeuwen, H. P., Eds.; Lewis, Boca Raton, FL, 1993; pp 118−163.
(22) Charlet L.; Manceau, A. *J. Colloid Interface Sci.* **1992**, *148*, 443.
(23) Chisholm-Brause, C. J.; O'Day, P. A.; Brown, G. E., Jr.; Parks, G. A. *Nature* **1990**, *348*, 528.
(24) Chisholm-Brause C. J.; Row, A. L.; Hayes, K. F.; Brown, G. E., Jr.; Parks, G. A.; Leckie, J. O. *Geochim. Cosmochim. Acta* **1990**, *54*, 1897.
(25) Fendorf, S. E.; Lamble, G. M.; Stapleton, M. G.; Kelley, M J.; Sparks, D. L. *Environ. Sci. Technol.* **1994**, *28*, 284.
(26) O'Day, P. A.; Parks, G. A.; Brown, G. E., Jr. *Clays Clay Miner.* **1994**, *42*, 337.
(27) O'Day, P. A.; Brown, G. E., Jr.; Parks, G. A. *J. Colloid Interface Sci.* **1994**, *165*, 269.
(28) Bleam, W. F.; McBride, M. B. *J. Colloid Interface Sci.* **1986**, *110*, 335.
(29) McBride, M. B. *Clays Clay Miner.* **1982**, *30*, 21.
(30) McBride, M. B.; Fraser, A. R.; McHardy, W. J. *Clays Clay Miner.* **1984**, *32*, 12.
(31) Evans, B. W.; Guggenheim, S. *Rev. Mineral.* **1988**, *19*, 225.
(32) Keren, R.; Grossl, P. R.; Sparks, D. L. *Soil Sci. Soc. Am. J.* **1994**, *58*, 1116.
(33) Russel, J. D.; Farmer, V. C.; Velde, B. *Min. Mag.* **1970**, *37*, 869.
(34) Carter, D. L.; Heilman, M. D.; Gonzalez, C. L. *Soil Sci.* **1965**, *100*, 356.
(35) Lamble, G. M.; Heald, S. M. *Rev. Sci. Instrum.* **1992**, *63*, 880.
(36) Stern, E. A.; Heald, S. M. *Rev. Sci. Instrum.* **1979**, *50*, 1579.
(37) Lytle, F. W.; Greegor, R. B.; Sandstorm, D. R.; Marques, E. C.; Wong, J.; Spiro, C. L.; Huffman, G. P.; Huggins, F. E. *Nucl. Instrum. Methods* **1984**, *226*, 542.
(38) Gurman, S. J.; Binsted, N.; Ross, I. *J. Phys. C* **1986**, *19*, 1845.
(39) Wieland, E.; Stumm, W. *Geochim. Cosmochim. Acta* **1992**, *56*, 3339.
(40) Wollast, R.; Chou, L. In *Physical and Chemical Weathering in Geochemical Cycles*; Lerman, A., Meybeck, M., Eds.; NATO ASI Series No. 251: Reidel: Dordrecht, The Netherlands, 1988; pp 11−32.
(41) O'Day, P. A.; Rehr, J. J.; Zabinsky, S. I.; Brown, G. E., Jr. *J. Am. Chem. Soc.* **1994**, *116*, 2938.
(42) Oswald, H. R.; Asper, R. In *Preparation and Crystal Growth of Materials with Layered Structures*; Lieth, R. M. A., Ed.; Reidel: Dodrecht, The Netherlands, 1977; pp 77−140.
(43) Manceau, A.; Combes, J. M. *Phys. Chem. Miner.* **1988**, *15*, 283.
(44) Combes, J. M.; Manceau, A.; Calas, G.; Bottero, J. Y. *Geochim. Cosmochim. Acta* **1989**, *53*, 583.
(45) Combes, J. M.; Manceau, A.; Calas, G. *Geochim. Cosmochim. Acta* **1990**, *54*, 1083.
(46) Lee, J. H.; Guggenheim, S. *Am. Mineral.* **1981**, *66*, 350.
(47) White, G. N.; Zelazny, L. W. *Clays Clay Miner.* **1988**, *36*, 141.
(48) Feitknecht, W. *Helv. Chim. Acta* **1942**, *25*, 555.
(49) Allmann, R. *Chimia* **1970**, *24*, 99.
(50) Taylor, R. M. *Clay Miner.* **1984**, *19*, 591.
(51) Charlet, L.; Manceau, A. *Geochim. Cosmochim. Acta* **1994**, *58*, 2577.
(52) Schenk, C. V.; Dillard, J. G. *J. Colloid Interface Sci.* **1983**, *95*, 398.
(53) Keren, R.; Sparks, D. L. *Soil Sci. Soc. Am. J.* **1995**, *59*, 430.
(54) Dzombak, A. D.; Morel F. M. F. *Surface Complexation Modeling*; John Wiley and Sons: New York, 1990; pp 43−64.
(55) Glushko, V. P. *Thermal constants of compounds*; Academy of Sciences: Moscow, USSR, 1972; Vol. 6, Parts 1 and 2.
(56) Sverjensky, D. A. *Rev. Mineral.* **1987**, *17*, 177.
(57) Shock, E. L.; Helgeson, H. C. *Geochim. Cosmochim. Acta* **1988**, *52*, 2009.
(58) Sverjensky, D. A. Johns Hopkins University, personal communication (OLI), 1988.
(59) Gurvich, L. V.; Veyts, I. V.; Alcock, C. B. *Thermodynamic properties of individual substances*; Bigell: New York, 1993.

Received for review May 1, 1995. Revised manuscript received August 29, 1995. Accepted August 30, 1995.[⊗]

ES950293+

[⊗] Abstract published in *Advance ACS Abstracts,* December 1, 1995.